Abatzoglou John (Orcid ID: 0000-0001-7599-9750)

Global Climatology of Synoptically-Forced Downslope Winds

John T. Abatzoglou[1,2*], Benjamin J. Hatchett[3], Paul Fox-Hughes[4], Alexander Gershunov[5], Nicholas J. Nauslar[6]

[1] University of California, Merced
Management of Complex Systems Department
jabatzoglou@ucmerced.edu
orcid.org/0000-0001-7599-9750
* corresponding author

[2]Department of Geography, University of Idaho, Moscow, ID

[3] Desert Research Institute, Reno, NV

[4] Bureau of Meteorology, Tasmania, Australia

[5] Scripps Institution of Oceanography, University of California, San Diego

[6] NOAA/NWS/NCEP Storm Prediction Center

Key Words: downslope winds, mountain meteorology

This is the author manuscript accepted for publication and has undergone full peer review but has not been through the copyediting, typesetting, pagination and proofreading process, which may lead to differences between this version and the Version of Record. Please cite this article as doi: 10.1002/joc.6607

Abstract: Downslope winds are mesoscale mountain meteorological phenomena that contribute to localized temperature extremes and can have numerous societal and environmental impacts. Whereas many previous studies have examined local downslope winds, no known efforts have attempted to identify and characterize meso- to synoptic-scale downslope winds globally using a common approach. We use a conceptual model for downslope winds that employs cross-barrier wind speed, near-mountain top static stability, and downward vertical velocity using thresholds guided by a chronology of local downslope winds and meta-analysis of downslope wind case studies. This approach was applied to ERA-5 reanalysis during 1979–2018 to develop a global atlas of downslope winds. Downslope winds adhered to distinct geographic and seasonal patterns, with peak occurrence in north-south oriented midlatitude mountains in the winter hemisphere associated with strong cross-mountain winds and stability. However, we identify numerous locations from the tropics to the high-latitudes where downslope winds occur at least 60 days a year as a byproduct of the general circulation and local-scale circulation interacting with topography. The four-decade-long dataset is also used to examine statistical relationships between the occurrence of downslope winds and El Niño-Southern Oscillation as well as long-term trends in downslope wind occurrence.

1. Introduction

Downslope winds are mesoscale mountain meteorological phenomena observed around the globe (Romanic, 2019; Bozkurt et al., 2018; Whiteman, 2000). The governing mechanisms of downslope winds are well-known and involve the interaction of synoptic flow with terrain that induces downward flow and transport of turbulent kinetic energy and subsequent adiabatic warming in the lee of a topographic barrier (Brinkmann, 1971; Elvidge & Renfrew, 2016). Strong winds and associated gusts accompanied by drying and warming through adiabatic compression and turbulent mixing can contribute to favorable conditions for rapid fire spread and are recognized as a critical fire weather pattern (Nauslar et al., 2018; Sharples et al., 2010; Westerling et al., 2004). Downslope winds can result in widespread impacts to infrastructure, ecosystems, public health, and transportation (Lawson & Horel, 2015; Delfino et al. 2009, Leibel et al., 2019). They also benefit wind energy production in some regions (Romanić et al., 2015). Finally, adiabatic warming associated with downslope winds contributes to extreme heat events (Nishi & Kusaka, 2019; Speirs et al., 2010) that pose impacts to society (Schwartz et al., 2020) and the cryosphere (van den Broeke, 2005; Cape et al., 2015; Speirs et al., 2010).

Downslope winds are a lower tropospheric to near-surface level manifestation of synoptically forced large-amplitude mountain waves (Durran, 1986; Smith, 1979). They are often associated with strong cross-barrier flow that accompanies either quasi-symmetric moist adiabatic ascent on windward and adiabatic descent on leeward slopes or leeward isentropic drawdown during periods of blocked flow (Sharples et al., 2010). Downslope winds arise from the interaction of synoptic forcing with terrain and although often displaying diurnal variability, they should be differentiated from diurnal terrain driven-flow associated with radiative cooling or convective outflows in quiescent synoptic conditions (Durran, 2003; Plavcan et al., 2014; Smith et al., 2018). Approaches to identify and forecast local-to-regional downslope winds have included: (i) cross-

barrier winds near mountaintop level, (ii) presence of stable layer or critical level at or above mountaintop level, (iii) cross-barrier sea level pressure gradient, and (iv) cross-barrier potential temperature gradient or downward sloping isentropes in the lee of a mountain barrier (Abatzoglou et al., 2013; Colle & Mass, 1998; Decker & Robinson, 2011; Lawson & Horel, 2015; Mercer et al., 2008; Romanić et al., 2016; Smith et al., 2018).

Numerous previous studies have identified and simulated meso- to synoptic-scale downslope wind events, but we are unaware of efforts that have attempted to generalize approaches globally. Prior work has highlighted some of the challenges in operationalizing objective approaches for identifying downslope winds due to nuances in mesoscale factors (e.g., Brinkmann, 1971). Yet, there is a need to develop scalable approaches to establish a global climatology of downslope wind events and to better understand their links to synoptic drivers, relationships with internal modes of climate variability, and their impacts. Some studies have identified regional downslope winds using surface observations (Plavcan et al., 2014; Smith et al., 2018), high-resolution model output (Guzman-Morales et al., 2016; Hughes & Hall, 2010), and global reanalysis (Montecinos et al., 2017). Station-based efforts have used temperature, humidity and winds, although deciphering the exact criteria for what constitutes downslope wind events is challenging even when stations are adequately located in mountainous environments (Mayr et al., 2018; Smith et al., 2018). High-resolution output from regional models should elucidate diagnostics for identifying downslope winds (e.g., downward vertical velocity, local acceleration of near-surface winds, and downward movement or overturning of isentropic surfaces), yet some studies suggest that <3 km horizontal model resolution is needed to adequately resolve their attributes (e.g., Cao & Fovell, 2016; Koletsis et al., 2009). However, previous studies have shown that a limited number of synoptic-scale diagnostics explain a vast majority of the occurrence and magnitude of regional downslope winds (Abatzoglou et al., 2013; Colle & Mass, 1998).

This study aims to develop a generalizable approach for identifying downslope winds globally using reanalysis data. The upshot of this effort is a first-known global climatology of meso- to synoptic-scale downslope wind events that may be used to better inform seasonal and geographic hazards posed by the phenomena, links to broader scale synoptic drivers, and relationships with internal modes of climate variability. We preface this by acknowledging that we do not propose to capture all downslope wind events or their magnitude. For example, some events may be not well-associated with synoptic drivers or resolved by the scale of the reanalysis products used. Instead, we aim for an approach that is guided by mountain wave and downslope windstorm theory and practice, performs well against existing regional downslope wind chronologies, and is scalable across numerical model products of varying resolutions.

2. Data and Methods

a. Datasets

Previous studies of regional downslope winds have used high-resolution model output (e.g., Guzman-Morales et al., 2016; Hughes & Hall, 2010; Koletsis et al., 2009). Such data would be ideal for developing a global climatology of downslope winds, but computational constraints currently limit the horizontal resolutions of multidecadal global reanalyses to >10 km. We use moderate horizontal resolution (~0.25°) global reanalysis data, the ERA-5 product from the European Centre for Medium Range Forecasts for the period January 1979–December 2018, to identify the potential for downslope winds. Advantages of ERA-5 over existing global reanalyses include advanced assimilation and parameterization procedures and enhanced spatial resolution (Hersbach & Dee, 2016). We acquired six-hourly (0Z, 6Z, 12Z, 18Z) pressure level data (1000–500hPa using a 50hPa vertical interval) of wind velocity, temperature, geopotential height, and

pressure vertical velocity (ω) globally from 80°S–80°N. While ERA-5 data is available hourly and at higher vertical resolution, we restrict our focus to more tractable scales.

A digital elevation model (DEM) from the Shuttle Radar Topography Mission (SRTM) was used to define topographic characteristics suitable for downslope flow. Data were further aggregated using geographic averages at 1/24° spatial resolution for computational efficiency and to constrain our focus to larger-scale landforms capable of enabling downslope wind events.

b. Methods

We first developed a static layer across global lands with terrain characteristics suitable to downslope flow. Quantitative approaches to identify mountains using DEM data exist (e.g., Korner et al., 2011), however, we are unaware of any widely-recognized topographic characteristics for downslope winds. Literature highlights the potential importance of cross-mountain asymmetry for the magnitude of downslope flow (Miller & Durran, 1991) and quasi-linear topographic barriers that limit around-barrier convergent flow (Markowski & Richardson, 2011). Given the lack of established terrain suitability for downslope winds, we consider the local terrain slope and elevational difference from mountaintop elevation. Herein, we defined mountaintop elevation as the maximum 1/24° elevation within a 50 km radius. Terrain slope was calculated at two different horizontal resolutions (1/24° and 1/4°) to maximize the potential suitability footprint. Suitable habitat for downslope winds was defined upon meeting two criteria: (i) local slope of at least 2%, and (ii) at least 200 m below mountaintop level. We further aggregate terrain suitability to the resolution of the ERA-5 grid (~25 km) and classify grids as suitable where at least 20% of 1/24° grid cells met criteria.

Approximately 25% of global lands between 80°N and 80°S met criteria for downslope wind suitability. There is some sensitivity of terrain suitability to these parameters (Figure S1). For example, 15% of global lands meet terrain suitability for slopes >4% and 32% for slopes >1% using a fixed >200m elevation below mountaintop level. Results showed nominal sensitivity to the choice of 20% of grid cells within an ERA-5 grid, with only 5% less land area being suitable if a stringent criterion of 60% was imposed. We opted for a liberal definition of terrain suitability as downslope winds have been observed across a broad portion of the globe, but emphasize that additional landform geometry (e.g., isolated mountain, length and width of mountain) are important in the surface manifestation and magnitude of downslope winds. These criteria are inherently subjective but are reasonably consistent with geographic locations of observed downslope winds (e.g., Figure S2; Table S1). Finally, while terrain suitability is defined as a static layer, dynamic meteorological fields determine where downslope wind events materialize at any given time.

We used a conceptual model for identifying downslope winds that considered three diagnostics: (i) cross-barrier wind near mountaintop level (v_{cb}), (ii) static stability ($\delta\theta/\delta Z$) at or above mountaintop level, and (iii) vertical velocity (ω) at or below mountaintop level (Figure 1a). Cross-barrier winds were calculated as the mean layer wind 0–100 hPa above mountaintop level orthogonal to the local gradient in terrain; maximum $\delta\theta/\delta Z$ was considered for the pressure surfaces 0–100 hPa above mountaintop level; and maximum ω was considered for all pressure surfaces from mountaintop level to ERA-5 ground level. We additionally considered the cross-barrier gradient in potential temperature, cross-barrier MSLP gradient, and near-surface wind velocity. Ultimately, we favored using the former set of diagnostics since those have been established by theoretical and modeling-based downslope wind research (Durran, 1986; Smith,

1985) and case studies (e.g., Lawson & Horel, 2015), and directly address the mechanisms of downslope winds (Durran, 2003).

Downslope winds were identified by the union of the three diagnostics exceeding thresholds in areas of suitable terrain. Rather than strictly require a collocated union of criteria, we allow for the potential for slight spatial displacement of features (e.g., the stable layer often occurs just upstream of the mountain barrier and downslope flow). Maximum cross-barrier winds and static stability were extended 60 km downwind to account for potential spatial offset in these features using an equilateral triangular polygon aligned to the direction of mountaintop winds (Figure 1b). The analysis hereafter focuses on the occurrence and climatology of downslope winds at loci of the aforementioned criteria. Yet, downstream extension of downslope winds is evident through shooting flows or hydraulic jumps (Hoinka, 1985), with transport of dust and smoke tied to these dynamics extending hundreds of kilometers downwind.

3. Selection and validation of criteria

Explicit validation of downslope wind events is confounded by the lack of agreed upon definitions, sparse monitoring networks in regions of complex topography, and lack of digital data from previously published regional downslope wind climatologies. In light of such challenges and to provide more robust support for identifying appropriate thresholds we used a paired validation effort that included a meta-analysis of published downslope wind events from across the globe and a chronology of regional downslope winds from southwestern California, USA. Furthermore, rather than presume a single set of thresholds for the three diagnostics, we evaluated the diagnostics across range of thresholds for v_{cb} (≥ 10 to ≥20 m s^{-1}, using 1 m s^{-1} increments), $\delta\theta/\delta Z$ (≥ 2 to ≥10 K km^{-1}, using 1 K km^{-1} increments), and ω (≥0.2 to ≥1.0 Pa s^{-1},

using 0.2 Pa s^{-1} increments) as a sensitivity analysis. Analyses herein serve as both a validation of our approach as well as to inform the selection of thresholds.

a. Case studies

We evaluated our diagnostic variables for 48 downslope winds events in the published literature designed to span geographic coverage of events post-2000 (Figure S2, Supplemental File). Evaluating these diagnostics across case studies serves to inform the selection of thresholds as well as to identify cases where diagnostics were inadequate. Many of these events were associated with impacts including fires (e.g., Nauslar et al., 2018) and infrastructure damage (Lawson & Horel, 2015).

We cataloged the approximate geographic location, date, and time (0Z, 6Z, 12Z, and 18Z) closest to the peak wind speed for each event (Table S3). This information was used to tabulate data on v_{cb}, and $\delta\theta/\delta Z$, and ω from ERA-5 at the closest grid cell. To reduce potential errors with the precise location and timing of events we cataloged the maximum values for ERA-5 grid cells directly adjacent to the grid cell and considered a temporal buffer of $\pm$ 6 hours.

Figure 2 provides an example of the diagnostic fields on 18Z 8 November 2018 across northern California. Strong northeasterly downslope winds across the northern Sierra Nevada facilitated the rapid spread of the Camp Fire near Paradise, California that burned 62,000 hectares, contributed to 85 fatalities, damaged nearly 19,000 structures, and resulted in severe air quality impacts on the densely populated coastal zone downwind. A broad area of strong downward ω is evident across the northern Sierra Nevada and coast ranges coincident with a strongly stable layer ($\delta\theta/\delta Z$>10 K km^{-1}) (Figure 2a). Winds at, and slightly above, mountaintop level were from

the east-northeast with v_{cb} > 20 m s^{-1} due east of Paradise, California (Figure 2b), consistent with weather station observations in the vicinity of the fire (Brewer & Clements, 2020).

Many commonalities were found among the three diagnostics considered for the case studies (Table S2; Figure S3). Approximately 80% of the events had $v_{cb} \geq 15$ m s^{-1}, with $v_{cb} \geq 25$ m s^{-1} for half of all cases. Around 80% of cases had moderately descending air ($\omega \geq 0.8$ Pa/s) with stronger descent ($\omega \geq 2.4$ Pa s^{-1}) present for half of the cases. Finally, over 90% of cases had a stable layer ($\delta\theta/\delta Z \geq 6$ K km^{-1}) with an isothermal or inversion layer ($\delta\theta/\delta Z \geq 10$ K km^{-1}) present for about half of the events.

Several events did not show evidence of the union of cross-barrier winds, downward motion, and stability per the conceptual model. These cases appeared for events that occurred in smaller-scale mountains where ERA-5 resolution may be inadequate, relatively short-lived events, or wind events more substantially influenced by diurnal flow characteristics and weakly coupled to synoptic forcing. Figure S4 provides a comparison of diagnostics for a Sundowner event that occurred on 6 May 2009 in south coastal California between ERA-5 output and 4-km output from a Weather Research and Forecasting (WRF) run for North America from 2001-2013 (Liu et al., 2017). ERA-5 output captures many of the broad scale features that would be identified as downslope winds per our criteria near the location of the Jesusita Fire that occurred. WRF provides additional nuance and shows that despite weaker cross-barrier winds (v_{cb} < 12 m s^{-1}) in smaller mountain ranges along the central coast of California, strong downward vertical velocity ($\omega \geq 2.4$ Pa s^{-1}) may be indicative of downslope winds (Figure S4). This suggests the scale of ERA-5 may be insufficient for capturing flow characteristics for smaller scale mountains.

b. Comparison to regional downslope wind chronologies

We used a complementary approach to evaluate the sensitivity of thresholds using a chronology of offshore Santa Ana wind events (SAW) in southwestern California that was developed by Abatzoglou et al., (2013) and extended through 2018 (Williams et al., 2019). This dataset identifies SAW from reanalysis data by the union of a sufficiently strong northeast gradient in MSLP and cold air advection at 850 hPa. This chronology exhibits strong relationships to extreme fire weather conditions from in-situ weather stations and other SAW chronologies (e.g., Guzman-Morales et al., 2016).

We calculated Heidke skill scores (HSS) as a validation of our conceptual model across a range of thresholds for v_{cb}, ω, and $\delta\theta/\delta Z$. HSS provides a measure of fractional improvement of a binominal forecast relative to a null case through the use of contingency tables where HSS=1 is a perfect forecast and HSS=0 represents no difference from a reference forecast or climatology. Whereas the SAW chronology catalogs synoptic drivers of offshore winds across broader southwestern California, the current approach is gridded and spatially explicit. To facilitate a more direct comparison between approaches, we first cataloged 6-hourly periods where at least 25% of the ERA-5 grid cells with suitable terrain in southern coastal California (32.5°–35.5°N, 115°–120°W) exceeded thresholds and mountaintop winds were from the northeast quadrant. Second, we account for differences in the temporal resolution of the SAW chronology (daily) and our approach (6-hourly) by requiring at least two of the four six-hour periods in a calendar day to meet the tested criteria. HSS were compared against a persistence-based reference forecast that used a 7-day time lag persistence to avoid entraining serial correlation as SAW events often last multiple days (e.g., Guzman-Morales et al., 2016).

Skill was highest (HSS>0.5) for intermediate levels of v_{cb}, ω, and $\delta\theta/\delta Z$ (Figure 3). Stringent thresholds result in a very low number of cases, whereas weaker thresholds resulted in numerous false negatives. We did not find strong evidence to suggest an optimal set of criteria, but rather that a range of intermediate thresholds was suitable for diagnosing SAW.

c. Selected thresholds for downslope winds

A large majority of the case study events and chronology of SAW occurred in a niche space consistent with our conceptual model. There is value in identifying an optimal set of criteria to diagnose a given phenomenon. This may be more achievable at local scales through parameterizations and incorporation of additional variables (e.g., Hughes & Hall, 2010) or alternatively using other empirical approaches and modeling techniques (Barbero et al., 2014).

Downslope winds were classified based on three criteria ($v_{cb} \geq 13$ m s^{-1}, $\omega \geq 0.6$ Pa s^{-1}, and $\delta\theta/\delta Z \geq 6$ K km^{-1}) contemporaneously being met at 6-hourly intervals. We constrained our focus to the number of days when at least two of the four 6-hourly intervals per day met the criteria to avoid short-lived episodes (e.g., Romanić et al., 2015). Forty-one of the 48 case studies met such criteria. Case studies that did not meet the criteria were typically deficient in a single criterion and plausibly were events with diurnal and thermodynamic drivers. These thresholds yielded HSS=0.5 in the SAW chronology. Notably, we found a reduced number of days (~18 days/year) meeting such criteria for offshore downslope winds in southwestern California compared to the SAW chronology (~30 days/year, Figure 3d) which likely reflects spatiotemporal differences in definitions. We additionally find a high interannual correlation (r=0.85) between the annual number of days meeting the criteria between the two approaches.

These thresholds are generally consistent with those in the literature. Durran (1990) and Whiteman (2000) suggest downslope winds can occur with $v_{cb} \geq 7$ m s^{-1} when strong stability exists near mountaintop level. Smith et al., (2018) suggested $v_{cb} \geq 10$ m s^{-1} while other regional studies suggest $v_{cb} \geq 15$ m s^{-1} for stronger downslope winds (e.g., Colle & Mass, 1998; Lawson & Horel, 2015). Studies rarely utilize ω as a diagnostic for downslope winds (Norte, 1988), but we contend that it should capture the conceptual model of the phenomena and is used by some operational forecasters for downslope winds. However, we acknowledge that our approach, as with many approaches for identifying meteorological phenomena, may be refined through the incorporation of additional parameters.

Explicit validation of such days meeting criteria in ERA-5 with in-situ observations is confounded by station siting, sparse observations near regions of complex terrain, and a lack of agreed upon diagnostics for quantifying downslope winds based on station data. We supplement the aforementioned validation using a limited set of hourly wind observations at three locations where downslope winds: (i) Fremont Canyon Remote Automated Weather Station, California, US, (ii) Perpignan–Rivesaltes Airport, Pepignan, France, and (iii) Fukushima Airport, Fukushima, Japan. Wind velocity is contrasted between days with downslope winds (at least 50% of suitable habitat within a 0.5° of each station meeting ERA-5 criteria) and days without any downslope winds. To avoid entraining seasonal biases in the latter, we exclude days in the calendar year that occurred more than 5 calendar days from any downslope wind. Comparative analyses with wind roses show distinct wind velocity characteristics for days with downslope winds across the three locations. Wind speeds were typically twice that on days with downslope winds than days without downslope winds and had distinct directional components. Fremont Canyon showed strong NE winds on days with downslope winds, characteristics of offshore Santa Ana winds (Figure 4b); Perpignan–Rivesaltes Airport showed a distinct strong NW wind characteristic of the

hybrid downslope-gap Tramontana winds on days with downslope winds (Figure 4d); Fukushima Airport showed strong N-NW flow on days with downslope winds (Figure 4f).

We examined the global distribution and seasonality of downslope winds as well as how this climatology qualitatively compares to previous efforts for a number of regional-to-continental scales. We additionally considered two supplemental research questions that explore temporal aspects of the data. First, we examined statistical relationships between the El Niño-Southern Oscillation (ENSO) and downslope wind occurrence during November–March, Spearman's rank correlation coefficients were calculated between the November–March average Multivariate ENSO Index (MEI, Wolter & Timlin, 2011) and the number of downslope wind days. Results were considered significant at $p<0.05$. Last, we examined linear trends in annual downslope wind occurrence during 1979-2018. Trends were calculated using Sen-Theil slope and considered significant using a two-tailed Mann-Kendall trend test at $p<0.05$.

4. Results

a. Climatology of downslope winds

Downslope winds were most prominent in the extratropics, particularly in the winter hemisphere, with local maxima in areas with prominent north-south oriented ranges collocated with strong zonal lower-tropospheric flow (Figure 5a). Local hotspots of downslope winds occurred in lands bordering the Southern Ocean, including the coast of Antarctica, as well as the southeastern portions of Greenland, which boast an average of 100 or more days per year meeting the criteria imposed. By contrast, downslope winds were less frequent (< 20 days per year) across most subtropical and tropical mountains.

The broad-scale climatology of downslope winds is strongly linked to the general circulation, namely the strength and location of the jet streams and lower-tropospheric stability (Figure 5b-

e). For example, the seasonal maximum in extratropical downslope winds occurs in winter with stronger lower-tropospheric winds and greater atmospheric stability. An exception was seen for islands and promontories in the Southern Ocean including New Zealand, Tasmania, and Tierra del Fuego where there is reduced seasonality in downslope wind frequency, consistent with persistent storm track activity. Climatologically weaker dynamics and reduced stability of tropical climates inhibit frequent downslope winds. A more detailed view of downslope wind climatologies for selected regional-to-continental scales is provided to elucidate local hotspots and to aid connecting our global atlas with local wind classification studies.

i. Western North America

The most prominent region of downslope winds occurred in the lee of the Rocky Mountains extending from southern Canada into the US where the conditions were met up to 100 days/year (Figure 6). These Chinook winds are most frequent in winter coinciding with the strongest dynamics (e.g., strong progressive westerly flow and larger MSLP gradients) and thermodynamic support (e.g., Whiteman, 2000). Other local maxima in downslope winds were seen across the Cascades, Sierra Nevada, the Pacific Ranges of British Columbia, the Peninsular and Transverse ranges of southern California, the Coast Ranges of northern California, northern Baja California, and the Sierra Madre Occidental of Mexico.

Maxima in downslope winds are often found on the east or northeast slopes of topographic barriers in western North America. This is consistent with prevailing cool season west-to-southwest lower-tropospheric winds. However, some exceptions are evident including along the western slope of the Wasatch Range, and offshore (easterly) winds can be found from the Cascades to the Coastal Ranges and Sierra Nevada of California (Reed, 1981). Downslope winds across southern California include both onshore winds (e.g., Evan, 2019) and offshore winds including SAW (Figure 3c), Diablo, and Sundowner winds. We find a similar climatology of

offshore downslope winds across southern California to previous Santa Ana wind approaches with a distinct peak in winter (Figure 3d, Abatzoglou et al., 2013; Guzman-Morales et al., 2016). The frequency of downslope winds was reduced in the summer across the region, with the primary exceptions being across the eastern slopes of the Cascades in Washington and Oregon and in the lee of prominent coastal capes in southern Oregon and northern California that experience strong northerly alongshore winds (Figure 6c).

ii. Australia and New Zealand

Central and eastern New Zealand are particularly susceptible to downslope winds due to their location within the austral westerly wind belt and the near north-south orientation of the Southern Alps (Figure 7, McGowan et al., 2002). The Canterbury Nor'wester on the south island of New Zealand is a common phenomenon throughout the year (McKendry, 1985). The flatter topography of northern and central Australia and less favorable circulation conditions in these regions limits downslope winds, but the Great Dividing Range of the eastern seaboard and mountainous island of Tasmania experience downslope winds at times. While most common in the winter (JJA), westerly winds and downslope flow can occur at any time of year (Fox-Hughes, 2012; Sharples et al., 2010). Suitable conditions for downslope winds also occurred over the northern Queensland tablelands, including occasionally as a consequence of tropical cyclones (Ramsay & Leslie, 2008).

The climatology resolves lesser known and studied downslope winds associated with the Flinders Ranges and Adelaide Hills of South Australia. These downslope winds were more common in the winter (JJA), but also contribute to the easterly Adelaide gully wind during the warm season (Sha, 1996). Also resolved is the easterly downslope wind of the Darling Scarp, just east of Perth, Western Australia. During the warmer months, downslope winds occur as the subtropical ridge

migrates to the south of the Australian continent and an inland thermal trough develops along the West Australian coast facilitating a localized MSLP gradient (Pitts & Lyons, 1989).

iii. Mediterranean

The mountainous region of southern Europe around the Mediterranean Basin experiences a winter (DJF) maximum in downslope wind frequency (Figure 8a). This is broadly evident for mountains across Spain (e.g., Pyrenees; Bougeault et al., 1990), Italy, Greece (e.g., Pelopónnisos; Koletsis et al., 2014), countries in the western Balkans in association with the Dinaric Alps, where northeasterly katabatic Bora Winds descend to the Adriatic (Belušić et al., 2013; Romanic, 2019), as well as eastern slopes of the Carpathian mountains of Romania and Ukraine. The Tramontane and Mistral winds of southern France appeared as a more seasonally persistent region of downslope winds with upwards of 40 days per year in DJF and 25 days per year in JJA. These winds following different topographic corridors generally arise from frequent strong Atlantic – Mediterranean MSLP gradients. They are squeezed and accelerated through topographic gaps on their descent to lower elevations (Obermann et al., 2018). The same synoptic patterns extend well into the Mediterranean driving downslope winds on the eastern slopes of the Corsican and Sardinian mountains hundreds of kilometers downwind.

The west coast of Turkey experiences summertime-accentuated downslope winds (Figure 8c), associated with northerly Etesian Winds in the Aegean Sea and further accentuated by daytime thermal lows forming over the Anatolian Plateau and an anticyclonic flow over the Balkans (Tyrlis & Lelieveld, 2013). These same flows also lead to frequent occurrence of summer (JJA) downslope winds in Crete (Koletsis et al., 2009b). The African side of the Mediterranean basin experiences mainly wintertime (DJF) downslope winds on the Atlas ranges of Morocco and Algeria and their eastern prolongation, the Aurès Mountains, stretching into Tunisia. Focal areas of frequent downslope winds in the summer (JJA) are evident on the coastal range of Libya as

well as ranges in Syria. Last, the characteristics of downslope winds are present year-round on topographic ranges bordering Gibraltar Strait (Dorman et al., 1995).

iv. South and Central America

The eastern slopes of the southern Andes and Patagonia had the greatest frequency of downslope winds due to their location near the southern hemisphere polar jet (Figure 9). For example, the Zonda is a warm, dry downslope wind along the eastern slopes of the Andes in the extratropical latitudes of South America peaking in winter (JJA) locally exceeding 40 days per winter (Antico et al., 2017; Norte, 1988). While westerly flow is predominant at these latitudes, offshore downslope winds also impact Chile (e.g., Puleche winds; Montecinos et al., 2017; Rutllant & Garreaud, 2004) primarily in the cool season.

Limited occurrence of downslope winds was seen in the tropics with the exception of the westward slopes of the central American Cordillera and the isthmus of Tehuantepec during DJF. Northerly downslope Tehuano gap winds (Hurd, 1929; Luna-Niño & Cavazos, 2018) are generated by cold fronts associated with transient surface highs that drop down from Canada, cross the Gulf of Mexico, and move over the Chivela Pass into the Gulf of Tehuantepec. Similar downslope-gap flow hotspots were also seen across western Costa Rica and Guatemala. In JJA there was an uptick in the occurrence of downslope winds coincident with the seasonally stronger trade winds across the Brazilian Highlands and a section of the Andean Cordillera stretching from northern Peru into Colombia.

v. East Asia

The mountains of Eastern Asia showed appreciable seasonal and latitudinal variability in downslope wind events with peak frequency in winter (DJF) north of the Himalaya (Figure 10). Local hotspots of downslope wind occurrence during the cool season were seen along the

eastern slopes of mountains in the Russian Far East, northern and southcentral China, the Japanese Alps (Kusaka & Fudeyasu, 2017), coastal Korea, Nepal, Bhutan, and the Truong Son Mountains between Vietnam and Laos. During spring, downslope winds are most frequent in the areas surrounding the Seas of Japan and Okhotsk.

Subtropical and tropical regions south of the Himalaya (~25°N) had more widespread downslope winds in summer (JJA) consistent with the flow reversal accompanying the Asian summer monsoon (Wang, 2002). Downslope winds during summer are notable in Vietnam, Laos, western Thailand, western Myanmar, and southcentral India (Figure 10c). Westerly downslope flow along the central coast plain of Vietnam has been used to signify the onset date of the monsoon, which also leads to a nadir in precipitation for this part of the country (Nguyen-Le et al., 2014). Though rare, extended summer downslope events have been observed in Japan (Inaba et al., 2002) and can occur in concert with tropical cyclones (Fudeyasu et al., 2008).

vi. Southern Africa

With the exception of the Atlas Mountains (see Mediterranean section), Madagascar, and South Africa, much of the African landmass does not experience frequent downslope wind events. This likely results from the remaining orography, particularly the mountains associated with the East African Orogen, being located within the tropics. Here, midlatitude disturbances that help establish synoptic pressure gradients, are infrequent and instability is much greater (e.g., Figure 5c). The primary areas subject to downslope winds are located in southern Africa (Figure 11) along the Atlantic coast in Namibia (Lancaster, 1985), along the periphery of South Africa, and across Madagascar with peak activity in winter (JJA).

Madagascar shows evidence of downslope winds being present throughout the year. A low-level jet associated with monsoonal circulation over the western Indian Ocean allows for strong flow

to interact with the elevated terrain of the region, most notably in JJA (Moore, 2013). Offshore Berg winds that occur from the Namib desert to South Africa are a well-known phenomenon (Lindesay & Tyson, 1990), as are downslope winds in southeastern portions of South Africa.

b. Relationships with ENSO

Widespread significant negative correlations between November–March MEI and the number of days of downslope winds were seen across the western US, most notably in the lee of the Cascades and Rocky Mountains (Figure 12a; statistically significant results shown in Figure S5a). By contrast, widespread positive correlations were seen across Mexico, Iran, and Arabia. This latitudinal dipole in downslope wind occurrence across the Americas is consistent with canonical patterns in the storm track and lower-tropospheric winds associated with ENSO. For example, zonal flow at near-mountaintop level (e.g., 700 hPa) across much of the northwestern US exhibits strong links to ENSO (Luce et al., 2013), with stronger west to southwest lower-tropospheric flow during La Niña conditions. We additionally highlight the dipole in downslope wind occurrence with ENSO across southern Australasia with positive correlations in Tasmania and New Zealand and negative correlations across the Great Dividing Range in southeastern Australia.

Correlations between MEI and downslope wind frequency reflects patterns seen in correlations between MEI and cross-barrier (primarily zonal) wind speed across much of the mid-latitudes (Figure S6a; L'Heureux & Thompson, 2006). Interannual variability in ω and $\delta\theta/\delta Z$ associated with ENSO may contribute to the occurrence of downslope winds as defined herein, but the broad-scale resemblance to lower-tropospheric wind speeds and specifically cross-barrier wind speeds is posited to exert a significant influence on regional interannual variability in downslope wind occurrence. In addition, preferred regional circulation regimes facilitating downslope winds

may be favored by ENSO phases as well as other climate modes (e.g. Guzman Morales et al., 2016).

c. Trends

While no statistically significant trend in global annual frequency in downslope wind occurrence was seen during 1979–2018, significant trends were evident in certain regions (Figure 12b; statistically significant results shown in Figure S5b). Increases in annual downslope wind activity occurred across the eastern slopes of the northern and central US Rocky Mountains, western slopes of the tropical Andes, the Kamchatka Peninsula, eastern South Africa, Brazilian Highlands, and Patagonia. Conversely, decreased occurrence of downslope winds were broadly seen across the Sierra Madre Occidental of Mexico, the Ural Mountains of Russia, and ranges across the countries of Iran, Afghanistan, and Pakistan. Trends in cross-barrier wind speeds (Figure S6b) show similarities to trends for downslope wind occurrence. Trends in annual downslope wind occurrence could obscure seasonal trends, as well as trends specifically tied to the direction of downslope winds in areas where downslope winds can occur on either side of a mountain barrier (e.g., California's Sierra Nevada).

Few studies have explicitly examined trends in the occurrence of downslope wind events. While studies have reported on widespread declines in near surface winds potentially linked to changes in surface roughness and large-scale circulation (McVicar et al., 2012; but see Zeng et al., 2019), the manifestation of such effects on distinct wind events is not well understood globally. Romanić et al., (2015) showed a decline in Koshava wind in the Balkans during 1949-2010. No significant trend has been seen in SAW in southern California to date (Guzman-Morales et al., 2016), although climate models project a decrease in SAW activity as a consequence of changing regional circulation patterns (Guzman-Morales & Gershunov, 2019).

5. Discussion and Conclusion

Our study provides a first known effort to identify downslope winds globally, complementing previous studies that have identified local-to-regional downslope winds. Whereas parameterized approaches for identifying local-to-regional downslope winds may provide additional detail and nuance, our climatologies generally mirror the climatological distribution of published studies. Moreover, the generalized approach developed herein allows for a seamless comparison of downslope winds across regions, including in regions where formal studies on downslope winds may be limited or non-existent.

While this study identified geographic locations of downslope winds, we do not further attempt to categorize the mesoscale dynamics associated with them. We envision typologies of downslope winds including: (1) adiabatic descent of progressive flow across terrain as is often observed with Chinook or Foehn winds (Oard, 1993), (2) the passage of a large-amplitude trough poleward of the location that facilitates isentropic drawdown complemented by cross barrier MSLP gradients (Hatchett et al., 2018), (3) trade-wind driven topographic hot spots further facilitated by tradewind inversions and gap flows (Schultz et al., 1997), and (4) passage of tropical disturbances over terrain (Tang et al., 2012). The influence of katabatic flow driven by horizontal temperature gradients and gap flows across terrain complement these dynamics and adds additional nuance into their seasonality, diurnal structure, and geographic hotspots (Amador et al., 2006; Hughes & Hall, 2010), some of which may not be adequately captured using the methodology used here.

We highlight several caveats and areas for improvement. First, our approach of identifying downslope winds on the union of three diagnostic variables from a conceptual model may overlook processes important to local downslope winds and makes no effort to quantify the

strength of the downslope winds themselves. Secondly, we make no effort to decouple the mesoscale effects of wind channeling through terrain itself (e.g., gap winds) which contribute to magnitude of downslope winds (Moritz et al., 2010). Thirdly, diurnally-driven downslope winds observed in parts of the globe (e.g., Zhong et al., 2008) will not be reflected in our analysis given the focus on synoptically-driven winds. Finally, our explicit use of ω likely biases our identification of downslope winds to spatial scales of topographically induced flow resolved by ERA-5. Aforementioned limitations in the resolution and physics of the ERA-5 global reanalysis product may limit elucidation of downslope winds at finer spatial scales. Spatial improvements in reanalyses and global climate models, as well as existing regional analyses, will provide additional detail to support our initial efforts.

We provide a publicly available database of downslope wind occurrence (location, date) and mountain top wind direction at http://climate.nkn.uidaho.edu/ACSL/DOWNSLOPEWINDS/. The database can motivate and guide more detailed and better resolved regional studies related to the occurrence and variability of downslope winds and their impacts. For example, the negative correlations between MEI and downslope winds dominating the mountainous western US likely are not indicative of relationships to the occurrence of offshore or northeasterly SAW of Southern California (Guzman-Morales et al., 2016), but rather those on the eastern slopes of north-south oriented mountains associated with progressive flow. We additionally encourage users of the database to further consider local topographic characteristics and station siting when trying to directly relate such information to local winds.

Distributed spatiotemporal information on downslope winds may aid in the understanding of a variety of impacts at local, regional, and global scales. Previous studies have demonstrated the importance of downslope winds to fire potential. Such events not only promote rapid desiccation of fuels, but also strong dry gusty winds facilitate rapid rates of spread of wildfires

that pose extreme hazards to communities located downwind and contribute to distinct regional fire regimes (e.g., Kolden & Abatzoglou, 2018; Westerling et al., 2004; Fox-Hughes et al., 2012). Strong downslope winds impose additional impacts on vegetation through windthrow as well as factors related to vegetation growth and establishment (Holtmeier & Broll, 2010). This suggests that such winds may factor into ecological niches identified globally. From a societal perspective, the seasonal and geographic distribution of downslope winds helps to identify potential risks to infrastructure and other wind-related hazards, including those tied to wind energy, power outages, transportation, and fire ignitions. Finally, meteorological downslope winds have also been shown to impact air quality (Aguilera et al., 2019; Li et al., 2015), and have association with an array of adverse effects to human health via entrainment and transport of dust (Evan, 2019), to smoke transport downwind of wildfires fanned by the same winds (Delfino et al., 2009, Leibel et al. 2019), and heat impacts on valley and coastal populations at the terminus of downslope winds (Schwartz et al., in review). Our database and conceptual model set the stage for evaluating downslope windstorm impacts and physical mechanisms, as well as plausible changes in downslope winds simulated by global models under a warming climate.

Acknowledgements: JTA was partially supported by the National Science Foundation under award DMS-1520873 and the Visiting Scholar Program and Fire Centre Research Hub at the University of Tasmania.

References

Abatzoglou, J. T., Barbero, R., & Nauslar, N. J. (2013). Diagnosing Santa Ana winds in Southern California with synoptic-scale analysis. *Weather and Forecasting*, *28*(3), 704–710.

Aguilera, R., A. Gershunov, S.D. Ilango, J. Guzman Morales and T. Benmarhnia, 2019: Santa Ana winds of Southern California impact PM2.5 with and without smoke from wildfires. *GeoHealth*, 4, e2019GH000225. https://doi.org/10.1029/2019GH000225.

Amador, J. A., Alfaro, E. J., Lizano, O. G., & Magaña, V. O. (2006). Atmospheric forcing of the eastern tropical Pacific: A review. *Progress in Oceanography*, *69*(2), 101–142.

Antico, P. L., Chou, S. C., & Mourão, C. (2017). Zonda downslope winds in the central Andes of South America in a 20-year climate simulation with the Eta model. *Theoretical and Applied Climatology*, *128*(1–2), 291–299.

Barbero, R., Abatzoglou, J. T., Steel, E. A., & Larkin, N. K. (2014). Modeling very large-fire occurrences over the continental United States from weather and climate forcing. *Environmental Research Letters*, *9*(12), 124009.

Belušić, D., Hrastinski, M., Večenaj, Ž., & Grisogono, B. (2013). Wind regimes associated with a mountain gap at the northeastern Adriatic coast. *Journal of Applied Meteorology and Climatology*, *52*(9), 2089–2105.

Bougeault, P., Clar, A. J., Benech, B., Carissimo, B., Pelon, J., & Richard, E. (1990). Momentum budget over the Pyrénées: The PYREX experiment. *Bulletin of the American Meteorological Society*, *71*(6), 806–818.

Brewer, J. M., & Clements, B. C. (2020). The 2018 Camp Fire: Meteorological Analysis Using In Situ Observations and Numerical Simulations. *Atmosphere*. 11, 47

Brinkmann, W. A. R. (1971). What is a foehn? *Weather*, *26*(6), 230–240.

van den Broeke, M. (2005). Strong surface melting preceded collapse of Antarctic Peninsula ice shelf. *Geophysical Research Letters*, *32*(12).

Campins, J., Jansa, A., Benech, B., Koffi, E., & Bessemoulin, P. (1995). PYREX observation and model diagnosis of the Tramontane wind. *Meteorology and Atmospheric Physics*, *56*(3–4), 209–228.

Cao, Y., & Fovell, R. G. (2016). Downslope windstorms of San Diego County. Part I: a case study. *Monthly Weather Review*, *144*(2), 529–552.

Cape, M. R., Vernet, M., Skvarca, P., Marinsek, S., Scambos, T., & Domack, E. (2015). Foehn winds link climate-driven warming to ice shelf evolution in Antarctica. *Journal of Geophysical Research: Atmospheres*, *120*(21), 11,11-37,57.

Colle, B. A., & Mass, C. F. (1998). Windstorms along the western side of the Washington Cascade Mountains. Part II: Characteristics of past events and three-dimensional idealized simulations. *Monthly Weather Review*, *126*(1), 53–71.

Decker, S. G., & Robinson, D. A. (2011). Unexpected high winds in northern New Jersey: A

downslope windstorm in modest topography. *Weather and Forecasting*, *26*(6), 902–921.
Delfino, R. J., Brummel, S., Wu, J., Stern, H., Ostro, B., Lipsett, M., et al. (2009). The relationship of respiratory and cardiovascular hospital admissions to the southern California wildfires of 2003. *Occupational and Environmental Medicine*, *66*(3), 189–197.
Dorman, C. E., Beardsley, R. C., & Limeburner, R. (1995). Winds in the Strait of Gibraltar. *Quarterly Journal of the Royal Meteorological Society*, *121*(528), 1903–1921.
Durran, D R. (2003). Downslope winds. Encyclopedia of Atmospheric Sciences, J. Holton, JA Curry, and J. APyle, Eds. Elsevier.
Durran, Dale R. (1986). Another Look at Downslope Windstorms. Part I: The Development of Analogs to Supercritical Flow in an Infinitely Deep, Continuously Stratified Fluid. *Journal of the Atmospheric Sciences*, *43*(21), 2527–2543.
Durran, Dale R. (1990). Mountain waves and downslope winds. In *Atmospheric processes over complex terrain* (pp. 59–81). Springer.
Elvidge, A. D., & Renfrew, I. A. (2016). The causes of foehn warming in the lee of mountains. *Bulletin of the American Meteorological Society*, *97*(3), 455–466.
Evan, A. T. (2019). Downslope Winds and Dust Storms in the Salton Basin. *Monthly Weather Review*, (2019).
Fox-Hughes, P. (2012). Springtime fire weather in Tasmania, Australia: Two case studies. *Weather and Forecasting*, *27*(2), 379–395.
Fudeyasu, H., Kuwagata, T., Ohashi, Y., Suzuki, S., Kiyohara, Y., & Hozumi, Y. (2008). Numerical study of the local downslope wind “Hirodo-Kaze” in Japan. *Monthly Weather Review*, *136*(1), 27–40.
Guzman-Morales, J., & Gershunov, A. (2019). Climate Change Suppresses Santa Ana Winds of Southern California and Sharpens Their Seasonality. *Geophysical Research Letters*.
Guzman-Morales, J., Gershunov, A., Theiss, J., Li, H., & Cayan, D. (2016). Santa Ana Winds of Southern California: Their climatology, extremes, and behavior spanning six and a half decades. *Geophysical Research Letters*, *43*(6), 2827–2834.
Hatchett, B. J., Smith, C. M., Nauslar, N. J., & Kaplan, M. L. (2018). Brief Communication: Synoptic-scale differences between Sundowner and Santa Ana wind regimes in the Santa Ynez Mountains, California. *Natural Hazards and Earth System Sciences*, *18*(2), 419.
Hersbach, H., & Dee, D. (2016). ERA5 reanalysis is in production. *ECMWF Newsletter*, p. Vol. 147, 7.
Hoinka, K. P. (1985). Observation of the airflow over the Alps during a foehn event. *Quarterly Journal of the Royal Meteorological Society*, *111*(467), 199–224.
Holtmeier, F.-K., & Broll, G. (2010). Wind as an ecological agent at treelines in North America, the Alps, and the European Subarctic. *Physical Geography*, *31*(3), 203–233.
Hughes, M., & Hall, A. (2010). Local and synoptic mechanisms causing Southern California’s Santa Ana winds. *Climate Dynamics*, *34*(6), 847–857.

Hurd, W. E. (1929). Northers of the Gulf of Tehuantepec. *Mon. Wea. Rev*, *57*, 192–194.

Inaba, H., Kawamura, R., Kayahara, T., & Ueda, H. (2002). Extraordinary persistence of foehn observed in the Hokuriku district of Japan in the 1999 summer. *Journal of the Meteorological Society of Japan. Ser. II*, *80*(4), 579–594.

Kolden, C. A., & Abatzoglou, J.T. (2018). Spatial Distribution of Wildfires Ignited under Katabatic versus Non-Katabatic Winds in Mediterranean Southern California USA. *Fire. 1, 19*

Koletsis, I., Lagouvardos, K., Kotroni, V., & Bartzokas, A. (2009a). Numerical study of a downslope windstorm in Northwestern Greece. *Atmospheric Research*, *94*(2), 178–193.

Koletsis, I., Lagouvardos, K., Kotroni, V., & Bartzokas, A. (2009b). The interaction of northern wind flow with the complex topography of Crete Island–Part 1: Observational study. *Natural Hazards and Earth System Sciences*, *9*(6), 1845–1855.

Koletsis, I., Kotroni, V., & Lagouvardos, K. (2014). A model-based study of the wind regime over the Corinthian Gulf. *Nat. Hazards Earth Syst. Sci.*, *14*(2), 459–472.

Kusaka, H., & Fudeyasu, H. (2017). Review of downslope windstorms in Japan. *Wind and Structures*, *24*(6), 637–656.

L'Heureux, M. L., & Thompson, D. W. J. (2006). Observed relationships between the El Niño–Southern Oscillation and the extratropical zonal-mean circulation. *Journal of Climate*, *19*(2), 276–287.

Lancaster, N. (1985). Winds and sand movements in the Namib sand sea. *Earth Surface Processes and Landforms*, *10*(6), 607–619.

Lawson, J., & Horel, J. (2015). Analysis of the 1 December 2011 Wasatch downslope windstorm. *Weather and Forecasting*, *30*(1), 115–135.

Leibel S., M. Nguyen, W. Brick, J. Parker, S. Ilango, R. Aguilera, A. Gershunov, T. Benmarhnia, 2019: Increase in Pediatric Respiratory Visits Associated With Santa Ana Wind-driven Wildfire and PM 2.5 levels in San Diego County. *Annals of the American Thoracic Society,* doi: 10.1513/AnnalsATS.201902-150OC.

Li, X., Xia, X., Wang, L., Cai, R., Zhao, L., Feng, Z., et al. (2015). The role of foehn in the formation of heavy air pollution events in Urumqi, China. *Journal of Geophysical Research: Atmospheres*, *120*(11), 5371–5384.

Lindesay, J. A., & Tyson, P. D. (1990). Thermo-topographically induced boundary layer oscillations over the central Namib, southern Africa. *International Journal of Climatology*, *10*(1), 63–77.

Liu, C., Ikeda, K., Rasmussen, R., Barlage, M., Newman, A. J., Prein, A. F., et al. (2017). Continental-scale convection-permitting modeling of the current and future climate of North America. *Climate Dynamics*, *49*(1–2), 71–95.

Luce, C. H., Abatzoglou, J. T., & Holden, Z. A. (2013). The missing mountain water: slower westerlies decrease orographic enhancement in the Pacific Northwest USA. *Science*, *342*(6164), 1360–1364.

Luna-Niño, R., & Cavazos, T. (2018). Formation of a coastal barrier jet in the Gulf of Mexico due

to the interaction of cold fronts with the Sierra Madre Oriental mountain range. *Quarterly Journal of the Royal Meteorological Society*, *144*(710), 115–128.

Markowski, P., & Richardson, Y. (2011). *Mesoscale meteorology in midlatitudes* (Vol. 2). John Wiley & Sons.

Mayr, G. J., Plavcan, D., Armi, L., Elvidge, A., Grisogono, B., Horvath, K., et al. (2018). The Community Foehn Classification Experiment. *Bulletin of the American Meteorological Society*, *99*(11), 2229–2235.

McGowan, H. A., Sturman, A. P., Kossmann, M., & Zawar-Reza, P. (2002). Observations of foehn onset in the Southern Alps, New Zealand. *Meteorology and Atmospheric Physics*, *79*(3–4), 215–230.

McKendry, I. G. (1985). An empirical and numerical modelling analysis of a complex meso-scale windfield, Canterbury Plains, New Zealand.

McVicar, T. R., Roderick, M. L., Donohue, R. J., Li, L. T., Van Niel, T. G., Thomas, A., et al. (2012). Global review and synthesis of trends in observed terrestrial near-surface wind speeds: Implications for evaporation. *Journal of Hydrology*, *416*, 182–205.

Mercer, A. E., Richman, M. B., Bluestein, H. B., & Brown, J. M. (2008). Statistical modeling of downslope windstorms in Boulder, Colorado. *Weather and Forecasting*, *23*(6), 1176–1194.

Miller, P. P., & Durran, D. R. (1991). On the sensitivity of downslope windstorms to the asymmetry of the mountain profile. *Journal of the Atmospheric Sciences*, *48*(12), 1457–1473.

Montecinos, A., Muñoz, R. C., Oviedo, S., Martínez, A., & Villagrán, V. (2017). Climatological characterization of Puelche winds down the western slope of the extratropical Andes Mountains using the NCEP climate forecast system reanalysis. *Journal of Applied Meteorology and Climatology*, *56*(3), 677–696.

Moore, G. W. K. (2013). Impact of the high topography of Madagascar on the structure of the Findlater Jet. *Geophysical Research Letters*, *40*(10), 2367–2372.

Moritz, M. A., Moody, T. J., Krawchuk, M. A., Hughes, M., & Hall, A. (2010). Spatial variation in extreme winds predicts large wildfire locations in chaparral ecosystems. *Geophysical Research Letters*, *37*(4), L04801.

Nauslar, N.J., Abatzoglou, J.T., & Marsh, P.T. (2018). The 2017 North Bay and Southern California Fires: A Case Study. *Fire, 1, 18.*

Nguyen-Le, D., Matsumoto, J., & Ngo-Duc, T. (2014). Climatological onset date of summer monsoon in Vietnam. *International Journal of Climatology*, *34*(11), 3237–3250.

Nishi, A., & Kusaka, H. (2019). Effect of foehn wind on record-breaking high temperature event (41.1° C) at Kumagaya on 23 July 2018. *SOLA*.

Norte, F. A. (1988). Características del viento Zonda en la Región de Cuyo. Facultad de Ciencias Exactas y Naturales. Universidad de Buenos Aires.

Oard, M. J. (1993). A method for predicting chinook winds east of the Montana Rockies. *Weather*

and Forecasting, *8*(2), 166–180.
Obermann, A., Bastin, S., Belamari, S., Conte, D., Gaertner, M. A., Li, L., & Ahrens, B. (2018). Mistral and Tramontane wind speed and wind direction patterns in regional climate simulations. *Climate Dynamics*, *51*(3), 1059–1076.
Pitts, R. O., & Lyons, T. J. (1989). Airflow over a two-dimensional escarpment. I: Observations. *Quarterly Journal of the Royal Meteorological Society*, *115*(488), 965–981.
Plavcan, D., Mayr, G. J., & Zeileis, A. (2014). Automatic and probabilistic foehn diagnosis with a statistical mixture model. *Journal of Applied Meteorology and Climatology*, *53*(3), 652–659.
Ramsay, H. A., & Leslie, L. M. (2008). The effects of complex terrain on severe landfalling Tropical Cyclone Larry (2006) over northeast Australia. *Monthly Weather Review*, *136*(11), 4334–4354.
Reed, R. J. (1981). A case study of a bora-like windstorm in western Washington. *Monthly Weather Review*, *109*(11), 2383–2393.
Romanic, D. (2019). Local winds of Balkan Peninsula. *International Journal of Climatology*, *39*(1), 1–17.
Romanić, D., Ćurić, M., Jovičić, I., & Lompar, M. (2015). Long-term trends of the 'Koshava' wind during the period 1949–2010. *International Journal of Climatology*, *35*(2), 288–302.
Romanić, D., Ćurić, M., Lompar, M., & Jovičić, I. (2016). Contributing factors to Koshava wind characteristics. *International Journal of Climatology*, *36*(2), 956–973.
Rutllant, J., & Garreaud, R. (2004). Episodes of strong flow down the western slope of the subtropical Andes. *Monthly Weather Review*, *132*(2), 611–622.
Schultz, D. M., Bracken, W. E., Bosart, L. F., Hakim, G. J., Bedrick, M. A., Dickinson, M. J., & Tyle, K. R. (1997). The 1993 superstorm cold surge: Frontal structure, gap flow, and tropical impact. *Monthly Weather Review*, *125*(1), 5–39.
Schwartz, L., Malig, B. J., Guzman Morales, J., Guirguis, K., Gershunov, A., Basu, R., & Benmarhnia, T. (2019). The health burden of fall, winter and spring heat waves in Southern California and contribution of Santa Ana Winds. *Proceedings of the National Academy of Sciences*, in review.
Sha, W. (1996). A numerical experiment on the Adelaide gully wind of South Australia. *Aust. Meteor. Mag.*, *45*, 19–40.
Sharples, J. J., Mills, G. A., McRae, R. H. D., & Weber, R. O. (2010). Foehn-like winds and elevated fire danger conditions in southeastern Australia. *Journal of Applied Meteorology and Climatology*, *49*(6), 1067–1095.
Smith, C., Hatchett, B. J., & Kaplan, M. (2018). A Surface Observation Based Climatology of Diablo-LikeWinds in California's Wine Country and Western Sierra Nevada. *Fire*, *1*(2).
Smith, C. M., Hatchett, B. J., & Kaplan, M. L. (2018). Characteristics of Sundowner Winds near Santa Barbara, California, from a Dynamically Downscaled Climatology: Environment and Effects near the Surface. *Journal of Applied Meteorology and Climatology*, *57*(3), 589–606.

Smith, R. B. (1979). The influence of mountains on the atmosphere. In *Advances in geophysics* (Vol. 21, pp. 87–230). Elsevier.

Smith, R. B. (1985). On severe downslope winds. *Journal of the Atmospheric Sciences*, *42*(23), 2597–2603.

Speirs, J. C., Steinhoff, D. F., McGowan, H. A., Bromwich, D. H., & Monaghan, A. J. (2010). Foehn winds in the McMurdo Dry Valleys, Antarctica: The origin of extreme warming events. *Journal of Climate*, *23*(13), 3577–3598.

Tang, X., Yang, M., & Tan, Z. (2012). A modeling study of orographic convection and mountain waves in the landfalling typhoon Nari (2001). *Quarterly Journal of the Royal Meteorological Society*, *138*(663), 419–438.

Tyrlis, E., & Lelieveld, J. (2013). Climatology and dynamics of the summer Etesian winds over the eastern Mediterranean. *Journal of the Atmospheric Sciences*, *70*(11), 3374–3396.

Wang, B. (2002). Rainy season of the Asian–Pacific summer monsoon. *Journal of Climate*, *15*(4), 386–398.

Westerling, A. L. AL, Cayan, D. R. D., Brown, T. T. J., Hall, B. L., & Riddle, L. G. (2004). Climate, Santa Ana winds and autumn wildfires in southern California. *Eos, Transactions American Geophysical Union*, *85*(31), 289–296.

Whiteman, C. D. (2000). *Mountain meteorology: fundamentals and applications*. Oxford University Press.

Williams, A. P., Abatzoglou, J. T., Gershunov, A., Guzman-Morales, J., Bishop, D. A., Balch, J. K., & Lettenmaier, D. P. (2019). Observed impacts of anthropogenic climate change on wildfire in California. *Earth's Future*. 7, 892– 910.

Wolter, K., & Timlin, M. S. (2011). El Niño/Southern Oscillation behaviour since 1871 as diagnosed in an extended multivariate ENSO index (MEI. ext). *International Journal of Climatology*, *31*(7), 1074–1087.

Zeng, Z., Ziegler, A. D., Searchinger, T., Yang, L., Chen, A., Ju, K., et al. (2019). A reversal in global terrestrial stilling and its implications for wind energy production. *Nature Climate Change*, *9*(12), 979–985.

Zhong, S., Li, J., Clements, C. B., De Wekker, S. F. J., & Bian, X. (2008). Forcing mechanisms for Washoe Zephyr—A daytime downslope wind system in the lee of the Sierra Nevada. *Journal of Applied Meteorology and Climatology*, *47*(1), 339–350.

Figure Captions

Figure 1: (a) Conceptual diagram for identifying synoptic conditions for downslope wind events. The mountaintop pressure level (P_2) is denoted by the bold dotted line as the pressure surface immediately above the mountain peak elevation. Cross-barrier wind speeds (v_{cb}) are calculated as the mean-layer cross-barrier wind speed 0–100hPa the mountaintop pressure level, the maximum $\delta\theta/\delta Z$ is calculated from 0–100hPa above mountaintop level, and maximum ω is considered from mountaintop level to nearest pressure level above ground level. "H" and "L" denote mean sea level pressure differences across the topography: relative high (H) and relative low (L). (b) Schematic for extending v_{cb} and $\delta\theta/\delta Z$ criteria downwind 60 km following an equilateral triangular polygon aligned to the direction of mountaintop winds. Downslope winds may be identified in downwind ERA-5 cells shown in grey as well as the originating cell on the basis of ω in the cell meeting criteria.

Figure 2: Downslope wind diagnostics on 18Z 8 November 2018 during the Camp Fire in northern California. Panels: (a) shows maximum ω (color, units of Pa s^{-1}) and maximum boundary layer $\delta\theta/\delta Z$ (small dots >6K km^{-1}, larger dots >10K km^{-1}), (b) v_{cb} (color, units of m s^{-1}) and mountain top wind velocity (vectors), and (c) pixels meeting criteria for downslope winds (brown); grey denotes region with suitable terrain. The location of the Camp Fire is denoted by the red star. Inset map in panel (c) shows context.

Figure 3: Matrix of Heidke Skill Scores (HSS) for using combinations of thresholds for (a) v_{cb} versus ω for $\delta\theta/\delta Z \geq 6$K km^{-1}, and (b) $\delta\theta/\delta Z$ versus ω for $v_{cb} \geq 13$ m s^{-1}. Panel (c) shows a wind rose diagram reflecting the directional distribution for downslope winds over all pixels in the red inset box (32.5–34.5°N, 115–117°W) for climatological seasons. The radial values indicate the percent of hours, with winds binned every 10°. For reference, the colors in the inset box show the percent of all 6-hour periods that met downslope wind criteria. Panel (d) compares the climatology of Santa Ana winds from the criteria used herein (blue) versus a previous climatology of Santa Ana winds (red) from Abatzoglou et al., (2013).

Figure 4: Wind roses for (left panels, a,c,e) days without downslope winds and (center panels, b,d,f) days with downslope winds for a majority of suitable terrain within 0.5° of three stations: (top) Fremont Canyon RAWS, US, Perpignan–Rivesaltes Airport, France (middle) , and (bottom) Fukushima Airport, Japan. Average hourly wind speed for both cases is shown in the title of each plot. Location of each station shown by the red star in the right panel with terrain for perspective.

Figure 5: (a) Annual average number of days where downslope criteria were met in at least two of four times in a calendar day during 1979-–2018. Areas in white were deemed not topographically suitable and omitted. Calculations were omitted for locations poleward of 80°. Zonal average fraction of suitable land showing the seasonal cycle with (a) identified downslope winds, (b) $v_{cb} \geq 13$ m s^{-1}, (c) $\delta\theta/\delta Z \geq 6$ K km^{-1}, and (d) $\omega \geq 0.6$ Pa s^{-1}. Summary statistics span the 1979-2018 period and were smoothed using a 21-day moving mean and 1-degree latitude moving mean. Latitudinal bands with no suitable land are shown in white.

Figure 6: Average annual number of days where downslope criteria were met in at least two of four times in a calendar day during 1979–2018 for (a) December-February, (b) March-May, (c) June-August, and (d) September-November. Areas in white were deemed not topographically suitable and omitted.

Figure 7: As in Figure 6 but for Australia and New Zealand.

Figure 8: As in Figure 6 but for the Mediterranean region.

Figure 9: As in Figure 6 but for South and Central America.

Figure 10: As in Figure 6 but for eastern Asia.

Figure 11: As in Figure 6 but for southern Africa.

Figure 12: (a) Spearman's rank correlation coefficient between November–March Multivariate ENSO Index and number of days with downslope winds during 1979–2018. (b) Linear trends in annual downslope wind occurrence during 1979–2018, in units of days per 40 years.

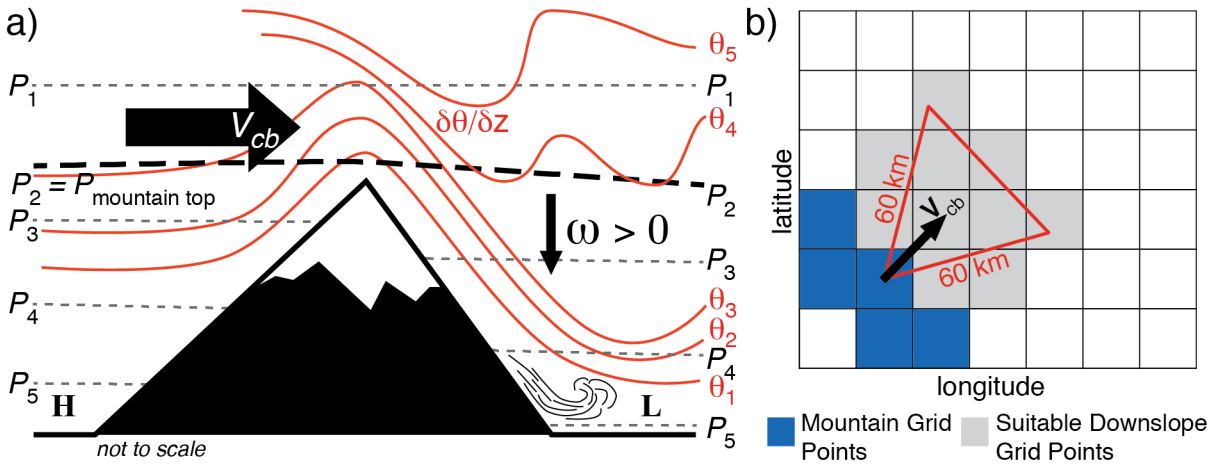

JOC_6607_fig1.tif

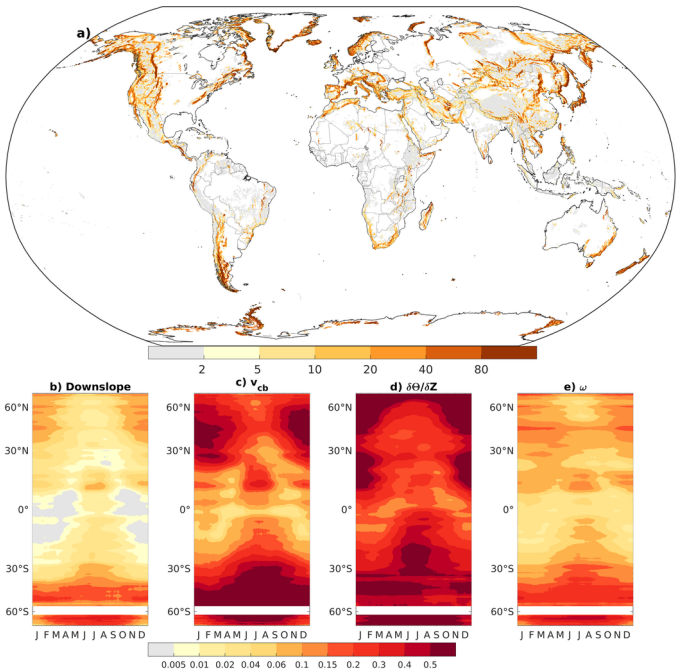

JOC_6607_fig5.tif

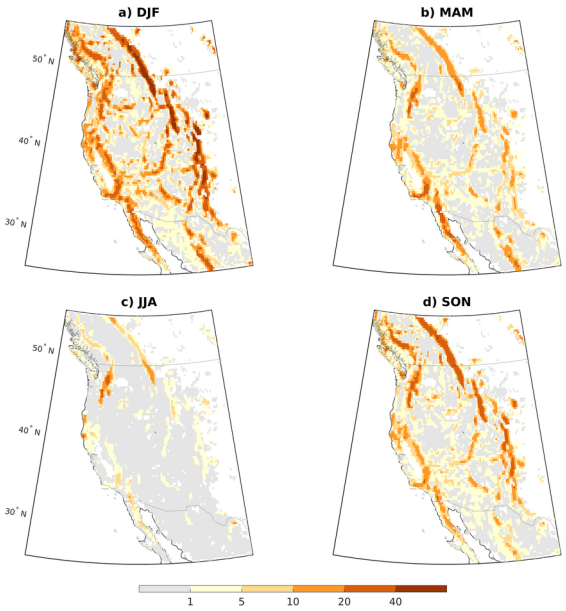

JOC_6607_fig6.tif

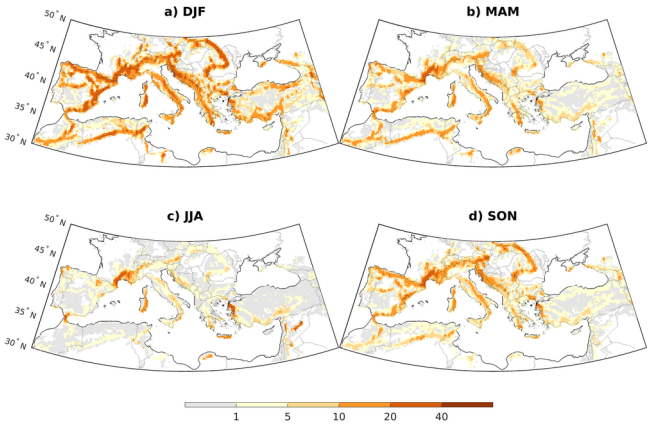

JOC_6607_fig7.tif

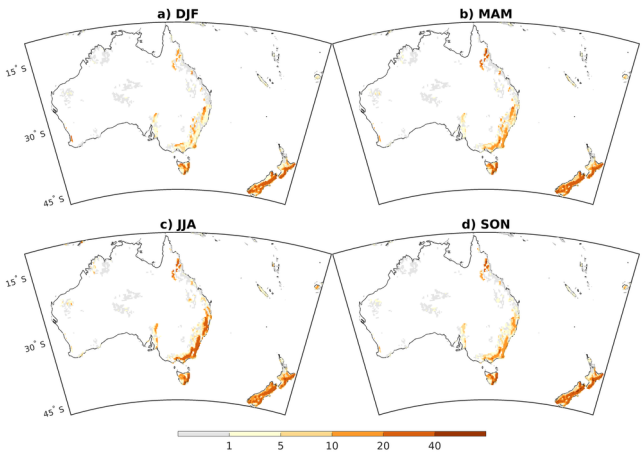

JOC_6607_fig8.tif

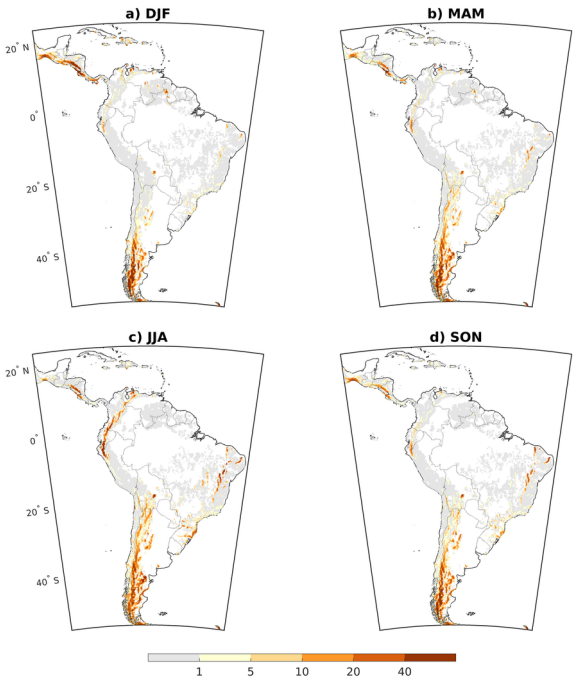

JOC_6607_fig9.tif

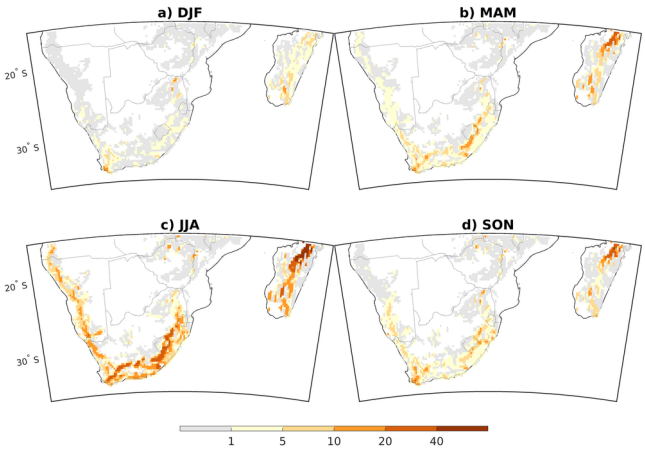

JOC_6607_fig10.tif

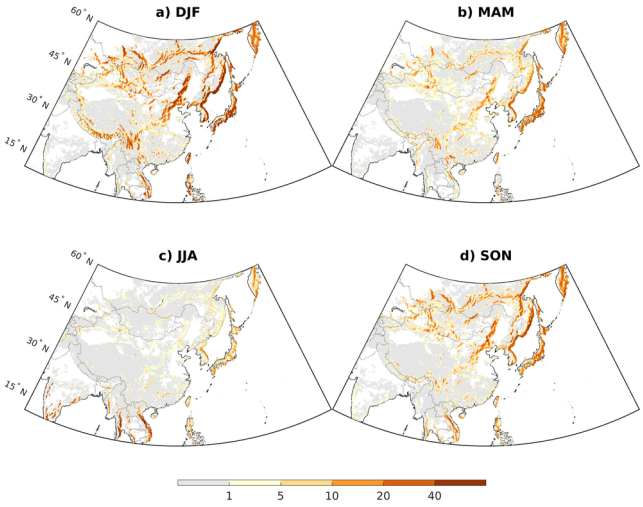

JOC_6607_fig11.tif

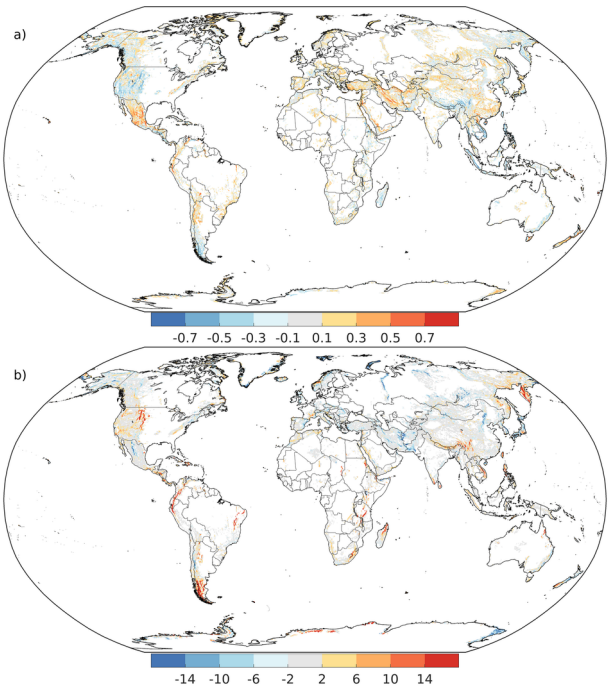

JOC_6607_fig12.tif

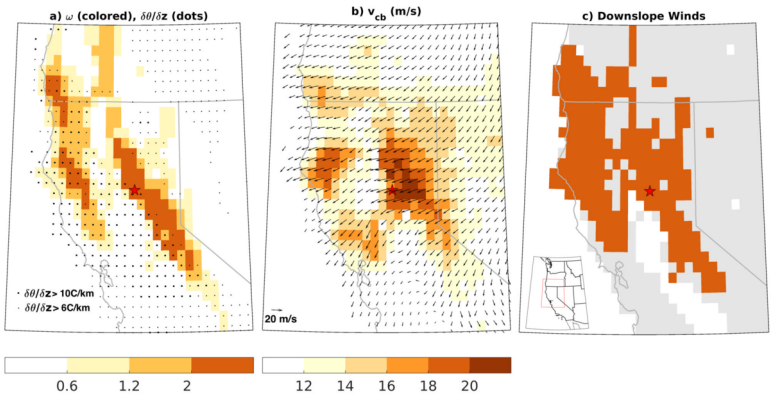

JOC_6607_FIG2.tiff

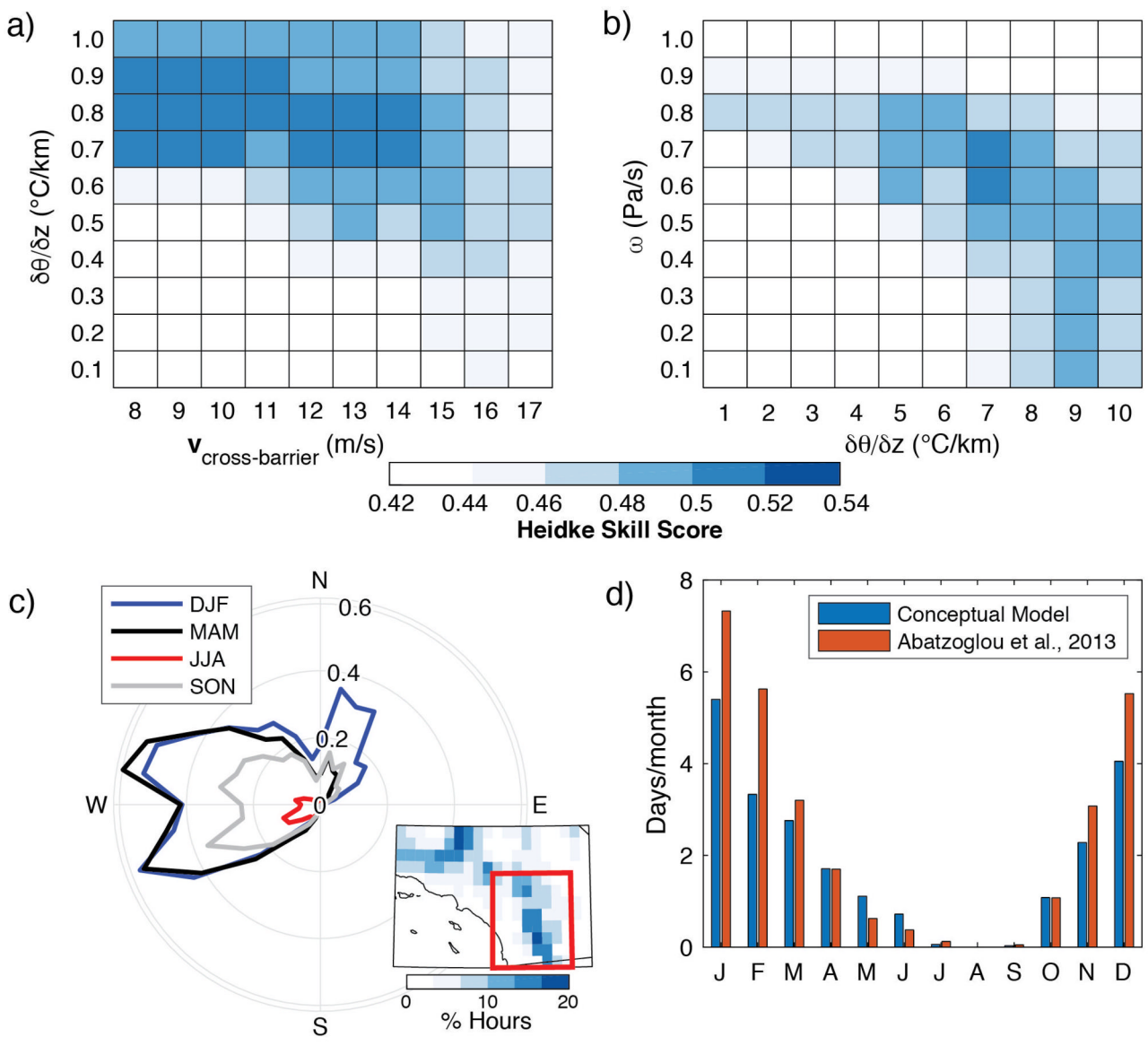

JOC_6607_FIG3.tiff

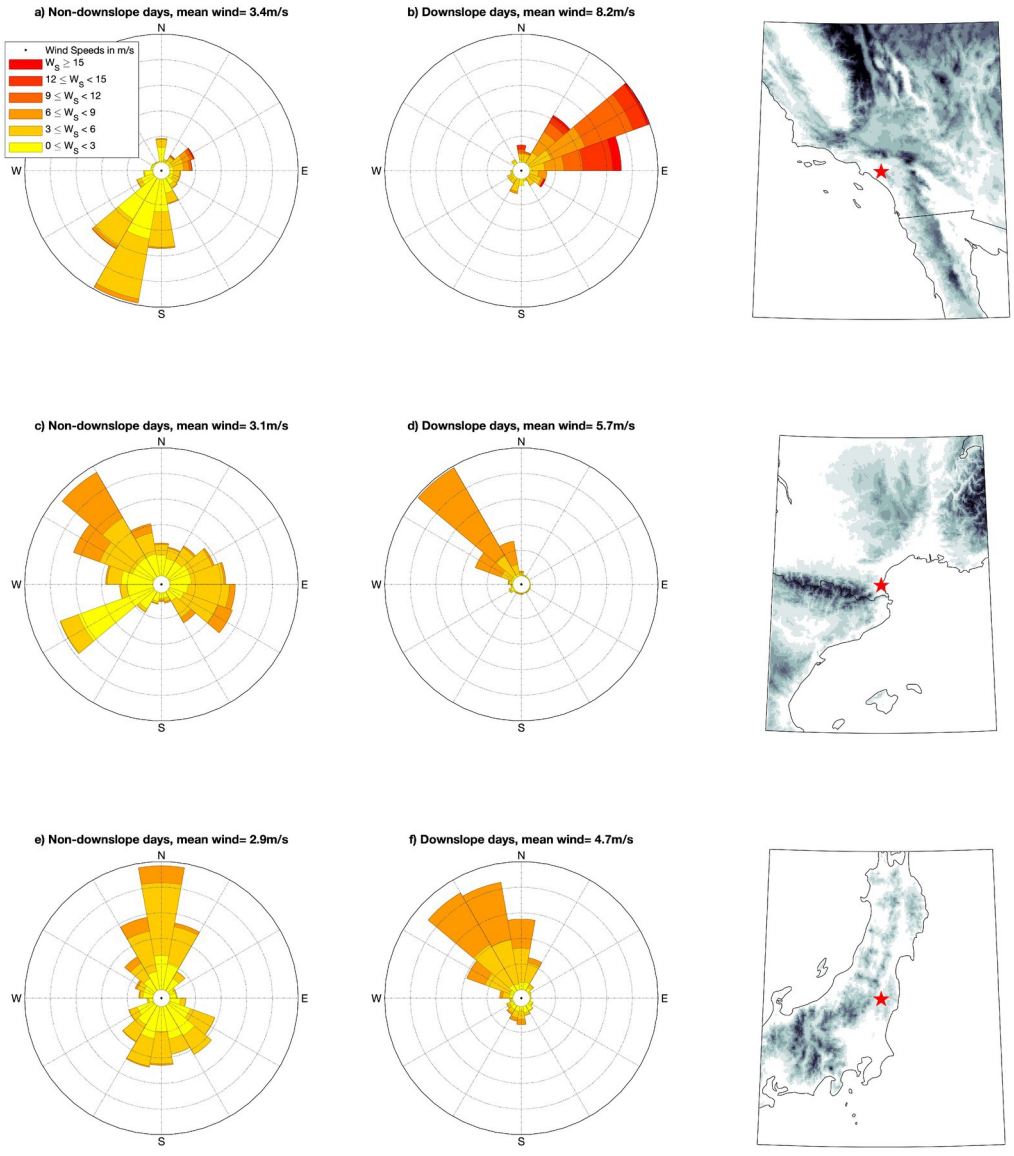

joc_6607_figure4.eps

Global Climatology of Synoptically-Forced Downslope Winds

John T. Abatzoglou*, Benjamin J. Hatchett, Paul Fox-Hughes, Alexander Gershunov, Nicholas J. Nauslar

Downslope winds can result in numerous impacts to human and natural systems. Understanding where and when these winds occur is of importance in to understand synoptic drivers and to better inform hazards posed by such winds. This study provides a first-known effort to develop a climatology downslope winds globally during 1979-2018.